THE ASTROPHYSICAL JOURNAL, 310:160–171, 1986 November 1

SMALL-SCALE VARIATIONS IN THE GALACTIC MAGNETIC FIELD: ROTATION MEASURE VARIATIONS ACROSS EXTRAGALACTIC RADIO SOURCES

J. H. SIMONETTI[1] AND J. M. CORDES[2]
Department of Astronomy, Cornell University; and the National Astronomy and Ionosphere Center
Received 1986 March 10; accepted 1986 April 18

ABSTRACT

In order to explore small angular scale ($\lesssim 1'$) variations in Faraday rotation measure through the interstellar medium, we have observed 26 mostly 3C and 4C extended extragalactic radio sources at four frequencies between 1300 MHz and 5000 MHz using the Very Large Array. Accurate rotation measures were sought for different components of each object to investigate the difference in rotation measure as a function of angular component separation. Such as analysis, essentially the computation of the structure function of rotation measure variations, can be interpreted using a power-law power spectrum for ($n_e \boldsymbol{B}$) variations in the interstellar medium, as presented in a previous paper. Sources were observed in three regions of the sky: (1) the north Galactic pole; (2) a region of large negative rotation measures just below the Galactic plane ($l^{\rm II} \approx 90°$, $b^{\rm II} \approx -30°$) called Region A by Simard-Normandin and Kronberg; and (3) through the Galactic plane at 90° Galactic longitude, just above Region A. For most sources, the rms difference in rotation measure between components is $\lesssim 10$ rad m^{-2} on angular scales $< 10'$. However, for the four sources in region (3) at $l^{\rm II} \approx 90°$, $|b^{\rm II}| < 10°$, we find ΔRM $\approx$ 50–100 on a $0'.1$–$1'$ scale, which argues for enhanced turbulence somewhere along the line of sight in this direction.

Subject headings: interstellar: magnetic fields — radio sources: general

I. INTRODUCTION

Investigations of the rotation measure (RM) on angular scales of degrees (linear scales of $\sim$1–100 pc for paths lengths through the Galaxy of $\sim$0.1–1 kpc), using observations of polarized extragalactic radio sources, have provided evidence for a large-scale systematic Galactic magnetic field and a smaller scale random component of roughly equal strength (e.g., Simard-Normandin and Kronberg 1980). Some work has been done on defining nearby structures in the interstellar medium, such as the "magnetic bubbles" of Vallée (1984), which may account for the large-scale ($\gtrsim$degrees) aspects of the random field. Comparatively little is known about the smaller scale variations which may be associated with turbulence in one or more phases of the interstellar medium. Theoretical discussions of isotropic magnetohydrodynamic turbulence in the various phases of the interstellar medium suggest turbulent length scales may range from $\sim$100 pc to $\lesssim$0.1 pc (Ruzmaikin and Shukurov 1982; McIvor 1977*a*, *b*). Observations of the interstellar scintillations of pulsars imply electron density variations at still smaller scales ranging from $\sim 10^{15}$ cm down to $\sim 10^{9}$ cm (Armstrong, Cordes, and Rickett 1981; Rickett, Coles, and Bourgois 1984; Cordes, Weisberg, and Boriakoff 1985). Higdon (1984) has suggested these observations are consistent with turbulence in a compressible, anisotropic gas where the anisotropy is due to the presence of a mean magnetic field. It is clear that much better observational constraints are needed to help identify the Galactic structure and physics of the random component.

In a previous paper (Simonetti, Cordes, and Spangler 1984, hereafter Paper I), we detailed a structure function approach for studying the small-scale (100–0.01 pc) variations in the Galactic magnetic field. Observations of RM variations across extended extragalactic radio sources, sensitive to variations on $\lesssim$arcmin scales, are the basis of such a study.

Where ψ is the observed position angle of linearly polarized radiation with wavelength λ, and ψ_0 is the initial position angle of the emitted radiation, the rotation measure RM is defined as

$$\psi - \psi_0 = \mathrm{RM}\ \lambda^2 \quad (1)$$

$$\mathrm{RM} = 0.81 \int_0^L n_e B_\parallel\, dl \ \mathrm{rad\ m^{-2}} \quad (2)$$

for path length L(pc), electron density n_e(cm^{-3}), and $B_\parallel$ (μG), the magnetic field component parallel to the line of sight. The structure function of the rotation measure is estimated by

$$\hat{\kappa}(\delta\theta) = N(\delta\theta)^{-1} \sum_{j,k} [\mathrm{RM}\ (\boldsymbol{\theta}_j) - \mathrm{RM}\ (\boldsymbol{\theta}_k)]^2 \ , \quad (3)$$

where the sum is over the $N(\delta\theta)$ observed sources whose angular separations $|\boldsymbol{\theta}_j - \boldsymbol{\theta}_k|$ are within a bin centered on $\delta\theta$. Model structure functions for the galactic RM assuming a power-law power spectrum for variations in the product $n_e \boldsymbol{B}$ are discussed in Paper I. Empirical structure functions are displayed in Paper I for three selected regions of the sky computed using rotation measures of extragalactic sources from the catalog of Simard-Normandin, Kronberg, and Button (1981) (angular separations $\gtrsim 5°$), and for a set of six extragalactic double sources from the literature (separation between components varying between $\sim 0°.01$ and $\sim 1°$).

In this paper we analyze observations of extended extragalactic radio sources to obtain more data on variations in Faraday rotation through the Galactic plane on angular scales $\lesssim$few arcmin. We have determined the difference in rotation measure (ΔRM) between components within 16 sources from observations using the Very Large Array. The resulting distribution of (ΔRM)^2 with component angular separation is basically consistent with the results presented in Paper I. The data also indicate there may be some strongly turbulent lines

[1] The National Radio Astronomy Observatory.
[2] Alfred P. Sloan Foundation Fellow.

of sight within the Galactic plane which may or may not be associated with localizable structures.

In § II we detail the observing procedure used, while a discussion of the data reduction is presented in § III. The results are discussed in § IV.

II. OBSERVATIONS

a) Source List

We attempted to investigate RM variations across sources within three regions of the sky: Region 1 ($85° < l^{II} < 115°$, $-40° < b^{II} < -10°$), an area of large, negative RMs at the heart of Simard-Normandin and Kronberg's (1980) Region A; the north Galactic pole (NGP, $b^{II} > 60°$); and various lines of sight through the galactic plane, in particular at $l° \approx 90°$, just above Region 1. Variations of RM on angular scales of degrees within Region 1 and the NGP were investigated in Paper I (see Fig. 10). Known double (or more complex) sources of large flux density were used and are listed in Table 1.

b) Observing Procedure

The observations were performed on 1982 September 6–7, using the "B" configuration of the VLA. To obtain accurate rotation measures (i.e., resolve the $n\pi$ position ambiguities), accurate position angles measurements were attempted at three frequencies in "*L*" band (1375, 1525, and 1675 MHz), and one frequency in "*C*" band (4885.1 MHz). The observing bandwidth was 50 MHz at *C* band, but 12.5 MHz was used at *L* band to reduce any Faraday-depolarization.

Integration times were ~ 5 minutes per frequency per source ("snapshots"), requiring a total intensity > 20 mJy beam^{-1} at each component peak (assuming 10% linear polarization) to obtain a precision of $< 10°$ in the position angle ψ at 20 cm. Typically, our sources were strong enough to lower the uncertainty to $\sigma_\psi \lesssim 3°$. These short integration times yield maps of relatively low dynamic range, but the source components are of approximately the same strength and we sought precision measurements at their peaks only. Some of the sources have widely separated components ($\gtrsim 1'$), and these were observed with two phase centers in *C* band to limit the effects of bandwidth smearing.

Amplitude and phase calibration of the array was accomplished by alternating on-source observations at each frequency with integrations on a nearby calibration point source. The source 0212+735 was observed for five periods throughout the 21 hr session for a total of ~ 15 minutes per frequency in order to calibrate the instrumental polarization. The source 3C 286 was used as a calibrator for the flux density scale and the absolute position angle (this source is observed to have zero rotation measure).

During the calibration stage, it was noticed that observations at 1675 MHz suffered from external interference during a few spaced intervals within the session. Therefore, some sources have no reliable data at that frequency, while due to the loss of some 0212+735 observations, position angles at 1675 MHz required special handling (see below).

III. DATA ANALYSIS

a) Map Production

The NRAO Astronomical Image Processing System (AIPS) was used to produce cleaned I_{tot}, Q, and U Stokes parameter maps of each of the sources. To enable accurate interfrequency comparisons for any particular source, final maps were produced with the same resolution at each frequency. This was accomplished either by convolving the cleaned maps with a two-dimensional Gaussian function chosen to compensate for the intrinsic differences in resolution at each frequency, or by utilizing the ability of the cleaning procedure to produce a final map of a chosen resolution. Finally, maps of polarized intensity $I_{pol} = [Q^2 + U^2]^{1/2}$, and position angle $\psi = \frac{1}{2}\tan^{-1}(U/Q)$ were constructed. As examples of the final products, total intensity maps at each frequency, with polarization vectors, of the sources 2203+292 and 2117+494 are shown in Figures 1–4. Fractional polarization at a given position was taken to be $m = I_{pol}/I_{tot}$, an accurate estimate when I_{pol} is large in comparison with the uncertainty in I_{pol}.

Uncertainties in the observed total intensity, $\sigma_{I_{tot}}$, and polarized intensity, $\sigma_{I_{pol}}$, were estimated by the rms fluctuation level in a region of the respective maps far from the source. These estimated uncertainties may be smaller than the actual uncertainties for measurements within the source. The uncertainty in position angle at a given location is estimated as $\sigma_\psi = \frac{1}{2}\sigma_{I_{pol}}/I_{pol}$, which is accurate at large I_{pol}.

b) Rotation Measures

We attempted to calculate RM for the pixel of peak polarized intensity within each independent emission region (i.e., isolated by a distance of more than one half-power synthesized beamwidth). Rotation measures were obtained from the slope of a linear least-squares fit of position angle ψ to λ^2, weighting data points by $1/\sigma_\psi{}^2$. Only frequencies where $I_{pol} > 3\sigma_{I_{pol}}$, and $m > 2\%$ were used in the fitting procedure. For a reduced χ^2 near unity, the squared uncertainty in RM was estimated by summing the $(\partial \mathrm{RM}/\partial\psi_i)^2\sigma_{\psi_i}{}^2$, or for large χ^2, computed using the variance of the ψ_i about the fitted line. Most sources we observed have separate components of strong enough polarization at each frequency to determine values of RM, while in some cases only one component is sufficiently polarized to allow a determination of RM (Table 1). Sources too weakly polarized to allow RM determinations are listed in Table 2.

The interference encountered at 1675 MHz reduced our ability to correctly calibrate the position angle at that frequency. In studying the NGP sources where RM is expected to be small, and those sources for which we had integrated RM values (i.e., averages over the whole source) from previous observations (Simard-Normandin, Kronberg, and Button 1981), we found ψ_{1675} to be systematically in error by $+40° \pm 6°$. Therefore, ψ_{1675} was corrected by this amount in all other sources before RMs were computed. We took the precaution of computing rotation measures with and without ψ_{1675}. The RMs from both methods agreed within their uncertainties.

Since position angle measurements are ambiguous by $n\pi$ radians we were not successful in obtaining unambiguous values of RM for the sources with $|\mathrm{RM}| \gtrsim 100$ rad m^{-2} given our spacing of observing frequencies. Potential fits to the data were searched for within a ± 500 rad m^{-2} range. Sources where difficulties were encountered are listed in Table 3 with their possible RMs. Where the galactic latitude is high and therefore $|\mathrm{RM}|$ is most probably small, we display the computed RM in Table 1. For sources where there exist previously observed RM values integrated over the entire source we were able to establish the RMs of the separate components. These latter sources are labeled by a footnote in Table 1. It is important to note that unless *a priori* integrated RM data are avail-

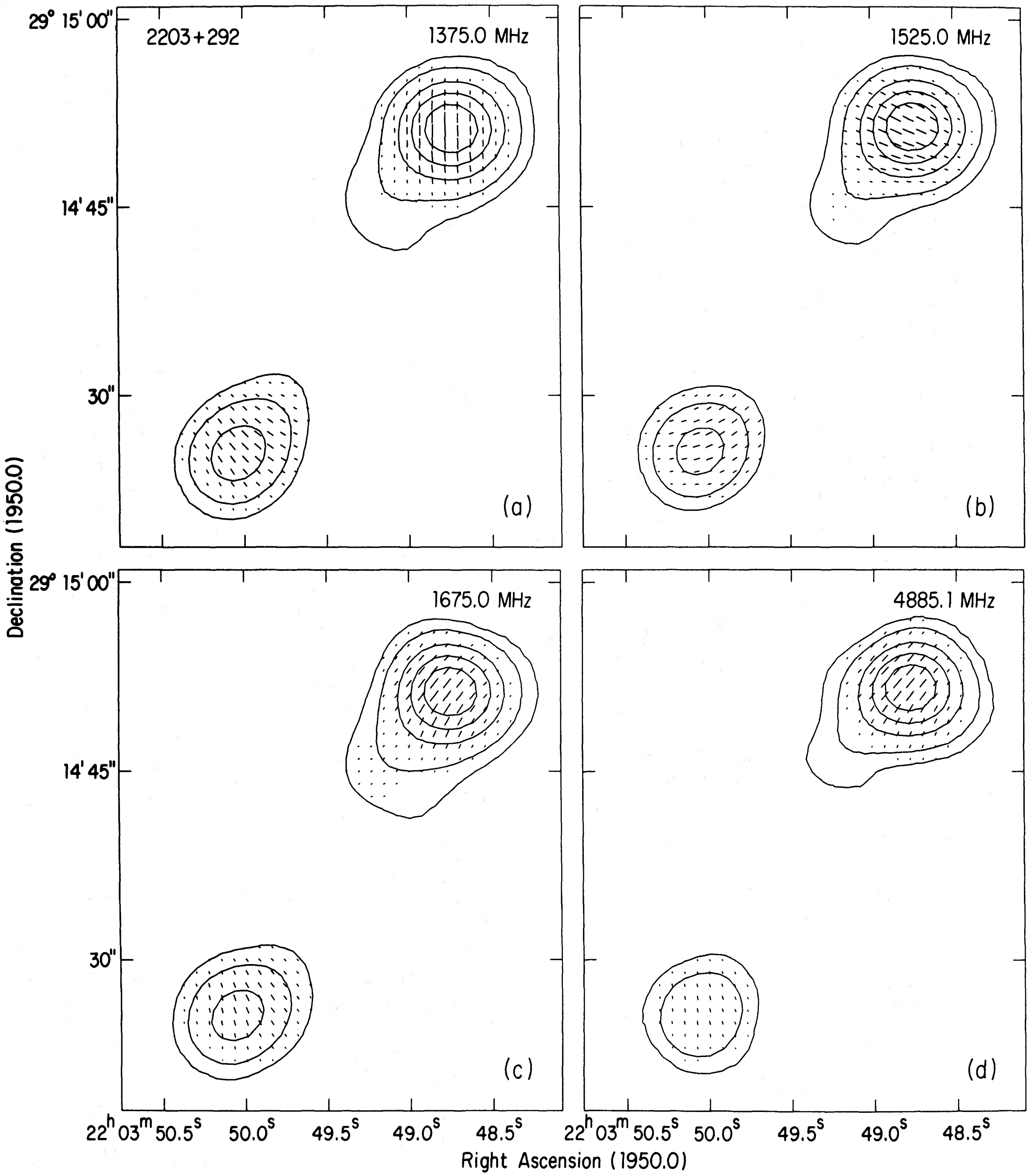

FIG. 1.—Maps at each frequency showing contours of total intensity (at 10, 20, 40, 60, and 80% of the peak intensity) with overlaid linear polarization vectors for the source 2203 + 292 ($|\Delta RM| = 2.8$ rad m^{-2}). The polarization position angles at 1675 MHz are as produced directly from the observational data, i.e., the systematic correction of § III*b* has *not* been applied in these maps. Peak total intensity and scale of the linear polarization vectors are (in units of mJy beam^{-1}, and mJy beam^{-1} arcsec^{-1}): (*a*) 969 and 90.7; (*b*) 850 and 88.3; (*c*) 793 and 75.7; and (*d*) 336 and 59.7.

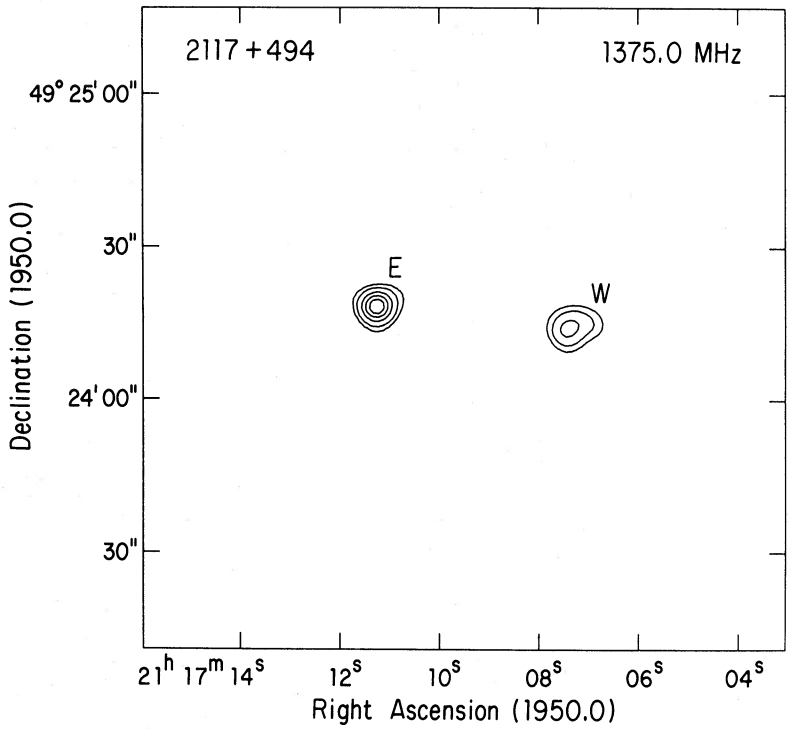

FIG. 2.—A total intensity map of the source 2117+494 at 1375 MHz ($|\Delta RM| = 59.5$ rad m^{-2}), showing the relative positions of the two components. Figs. 3 and 4 display the polarization information for the separate components (E and W).

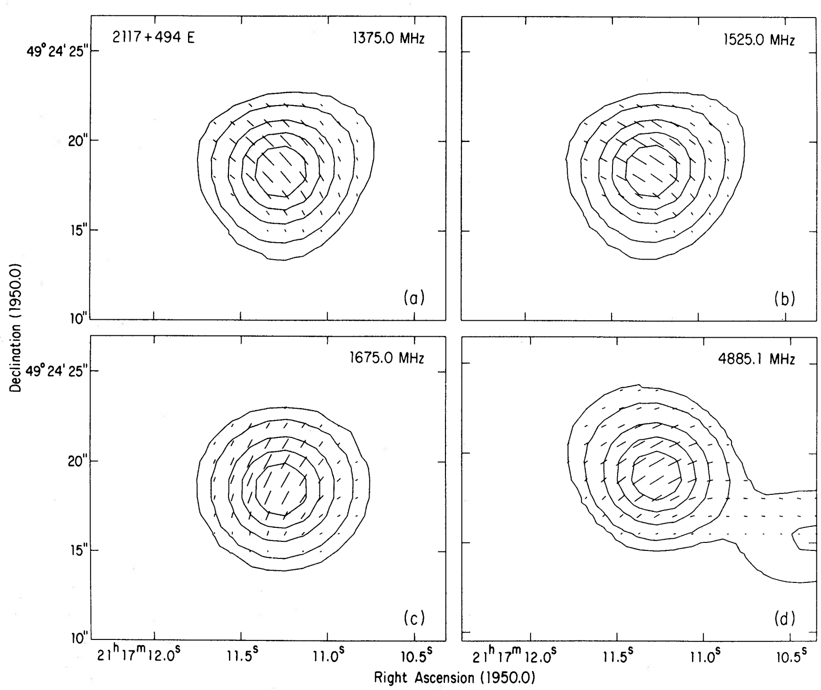

FIG. 3.—As in Fig. 1, for the E component of 2117+494. Peak total intensity and scale of the linear polarization vectors are (mJy beam^{-1}, and mJy beam^{-1} arcsec^{-1}): (*a*) 1656 and 167; (*b*) 1424 and 134; (*c*) 1224 and 119; and (*d*) 399 and 38.9.

TABLE 1

FARADAY ROTATION MEASURES

Source[a]	3C/4C	l^{II}	b^{II}	Region[b]	R.A.(1950.0)	Decl.(1950.0)	m_L/m_C[c]	RM[d] (rad m^{-2})	$\delta\theta$[e] (″)	ΔRM (rad m^{-2})
1218+339(1)[f]	270.1	166°3	80°6	NGP	12ʰ18ᵐ03ˢ9	33°59′46″	0.49(0.03)	1.5(0.5)	...	...
1232+216(1)[f]	274.1	269.8	83.1	NGP	12 32 53.6	21 36 46	1.23(0.3)	−3.9(1.2)	...	...
(2)					12 33 02.3	21 37 27	1.5 (0.3)	−4.6(1.7)	...	...
(1−2)									141	0.7(2.1)
1241+166(1)[f]	275.1	293.4	79.1	NGP	12 41 27.3	16 39 26	0.96(0.14)	−10.7(1.0)	...	...
(2)					12 41 27.6	16 39 12	0.30(0.05)	−8.5(3.5)	...	...
(1−2)									15	−2.2(3.6)
1251+278(1)[f]	277.3	72.0	89.2	NGP	12 51 46.2	27 53 38	0.95(0.04)	6.1(1.3)	...	...
(2)					12 51 46.5	27 53 56	0.60(0.19)	3.6(5.9)	...	...
(1−2)									18	2.5(6.0)
1308+277(1)[f]	284.0	38.5	85.6	NGP	13 08 34.1	27 44 17	0.82(0.41)	−2.4(1.7)	...	...
(2)					13 08 46.7	27 43 47	1.0 (0.15)	−1.0(0.6)	...	...
(1−2)									170	−1.4(1.8)
1323+370(1)	37.38	88.0	77.9	NGP	13 23 45.9	37 03 47	1.1 (0.5)	6.6(2.0)	...	...
(2)					13 23 46.4	37 03 41	0.68(0.17)	3.7(1.3)	...	...
(3)					13 23 46.8	37 03 30	1.5 (0.5)	4.3(1.5)	...	...
(1−2)									8	2.9(2.4)
(2−3)									12	−0.6(2.0)
(1−3)									20	2.3(2.5)
0007+332(1)	33.01	113.2	−28.6	1	00 07 49.8	33 12 15	1.3 (0.3)	...	...	...
(2)					00 07 50.2	33 13 30	0.96(0.03)	...	...	...
(1−2)									75	4.8(1.3)
0017+257(1)	25.01	114.1	−36.3	1	00 17 02.6	25 45 51	1.02(0.16)	...	...	...
2153+377(1)	438.0	88.8	−13.0	1	21 53 45.1	37 46 18	>4.5[h]	...	...	...
(2)					21 53 45.1	37 46 07	>4.5[h]	...	...	...
(1−2)									16	−1.4(1.9)
2203+292(1)[f]	441.0	84.9	−20.9	1	22 03 48.8	29 14 51	0.55(0.01)	−128.6(3.6)	...	...
(2)					22 03 50.0	29 14 26	0.85(0.01)	−131.2(1.2)	...	...
(1−2)									30	2.6(3.8)
2239+333(1)	33.57	94.1	−21.9	1	22 39 08.0	33 21 28	0.56(0.11)	...	...	...
2244+366(1)[f]	36.47	96.8	−19.5	1	22 44 12.6	36 40 39	0.55(0.15)	−245.0(2.1)	...	...
(2)					22 44 13.0	36 40 45	0.52(0.17)	−219.9(2.5)	...	...
(1−2)									8	−25.1(3.3)
2251+379(1)	37.67	98.8	−19.1	1	22 51 33.6	37 55 27	1.1 (0.20)	...	...	...
(2)					22 51 37.3	37 53 59	0.83(0.04)	...	...	...
(1−2)									98	−10.6(1.4)
2349+327(1)	32.69	108.9	−28.2	1	23 49 48.4	32 47 44	0.88(0.11)	...	...	...
(2)					23 49 48.8	32 47 22	1.17(0.12)	...	...	...
(3)					23 49 50.2	32 46 49	1.02(0.12)	...	...	...
(1−2)									23	1.8(2.0)
(2−3)									38	2.0(1.4)
(1−3)									60	3.9(0.8)
2353+283(1)	28.59	108.4	−32.7	1	23 53 21.1	28 19 14	1.0 (0.1)	...	...	...
2106+494(1)[f]	428.0	90.5	1.3	P	21 06 40.6	49 24 52	1.19(0.31)	−361.6(1.3)	...	...
(2)					21 06 43.0	49 24 09	0.24(0.05)	−281.8(6.1)	...	...
(1−2)									49	−79.8(6.2)
2111+620(1)[g]	429.0	100.3	9.4	P	21 11 39.1	62 02 34	0.56(0.14)	−247.0(22.2)	...	...
(2)					21 11 40.0	62 02 38	1.2 (0.5)	−198.5(11.3)	...	...
(1−2)									7	−48.5(24.9)
2117+605(1)	430.0	99.7	8.0	P	21 16 59.2	60 34 55	0.66(0.05)	...	...	...
(2)					21 17 05.6	60 36 05	1.43(0.21)	...	...	...
(1−2)									84	92.8(3.7)
2117+494(1)[f]	431.0	91.7	0.1	P	21 17 07.2	49 24 16	1.40(0.6)	386.2(2.7)	...	...
(2)					21 17 11.2	49 24 19	1.14(0.21)	326.9(1.3)	...	...
(1 − 2)									39	59.4(3.0)
1753−113(1)	...	16.4	6.9	0	17 53 03.9	−11 19 56	0.63(0.3)	...	...	...
(2)					17 53 04.8	−11 19 42	1.01(0.3)	...	...	...
(1−2)									19	−6.2(4.0)
1954+331(1)	...	69.5	2.5	0	19 54 16.7	33 10 38	1.12(0.3)	...	...	...

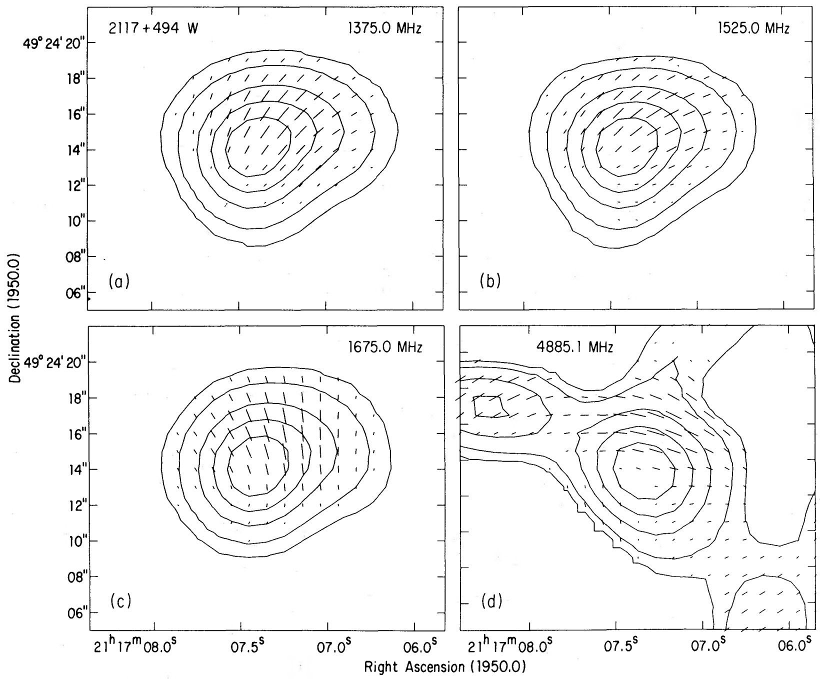

FIG. 4.—The W component of 2117+494. Peak total intensity and scale of the linear polarization vectors are (mJy beam^{-1}, and mJy beam^{-1} arcsec^{-1}): (*a*) 821 and 91.8; (*b*) 733 and 74.6; (*c*) 633 and 66.4; and (*d*) 240 and 16.7.

able, or the observed set of frequencies includes a few sufficiently closely spaced values, it is difficult to overcome $n\pi$ position angle ambiguities. Choosing the RM which yields the smallest χ^2 *may not* give the correct result since actual deviations from a linear ψ versus λ^2 law can lead to the rejection of the actual RM value.

While absolute rotation measures were not obtainable for each source, differences in RM between each component were easily derived in many cases. Where ΔRM could not be calculated using RMs for each component, we relied upon a fit of the *difference* in position angle between two components to λ^2 to get ΔRM. This worked well, and results derived by either method for the sources with known component RMs were consistent. (Note that if the second method is used, then any previous correction to ψ_{1675} for systematic error does not affect the calculation of ΔRM.) In two cases (2117+605, and 2251+379) the ΔRM values calculated through a fit to the difference in ψ between the components seemed unreliable as a result of a possible $n\pi$ ambiguity. For these sources, we used the intercomponent differences in the sets of possible RMs to compute ΔRM (see Table 3). That the resulting large ΔRM is reasonable for 2117+605 is confirmed by observations by Spangler, Myers, and Pooge (1984). For completeness, the position angles and other relevant parameters for all sources are shown in Table 4. Figures 5–9 display ψ versus λ^2 fits for a source with small ΔRM, and the four sources near the galactic plane with large ΔRM.

TABLE 2

WEAKLY POLARIZED SOURCES (NO ROTATION MEASURE DETERMINED)

Source	Polarization[a]
1336+391 (3C 288.0)	unpolarized
1841−015	unpolarized in *L* band
1847−016	unpolarized in *L* band
2012+234 (3C 409.0)	unpolarized
2325+269 (4C 27.52)	unpolarized

[a] "Unpolarized" means percentage polarization $\lesssim 1\%$.

IV. RESULTS AND DISCUSSION

In Figure 10 we display the observed $(\Delta\mathrm{RM})^2$ for each pair of components for each source in Table 1. Only independent

NOTES TO TABLE 1

[a] Polarized source components are labeled by (1), (2), etc. The component difference in RM (ΔRM) is on the row labeled, for example, by (1−2). Note some sources have only one polarized component.

[b] NGP, and Region 1 defined in text. *P* sources are at $l^{\mathrm{II}} \approx 90°$, $|b^{\mathrm{II}}| < 10°$; sources labeled "0" are in the galactic plane, but not near $l^{\mathrm{II}} \approx 90°$.

[c] The ratio of the polarization percentage at 20 cm to that at 6 cm. Uncertainties in parentheses.

[d] Given only where all $n\pi$ position angle ambiguities were resolved; see Table 2 for sources which have no entry here.

[e] Component separation.

[f] Simard-Normandin, Kronberg, and Button 1981 integrated RM values: 1218+339 RM = 0(0.4); 1232+216 RM = −4(0.3); 1241+166 RM = −11(1); 1251+278 RM = 3(1); 1308+277 RM = −4(1); 2203+292 RM = −125(1); 2244+366 RM = −231(3); 2106+494 RM = −359(1); 2117+494 RM = 347(3) rad m^{-2}.

[g] Vallée 1983 integrated RM value: 2111+620 RM = −208(2) rad m^{-2}.

[h] Fractional polarization at 4885.1 MHz for 2251+378 is <1%.

TABLE 3

SOURCES WITH AMBIGUOUS ROTATION MEASURE

SOURCE	POSSIBLE RM VALUES[a] (rad m^{-2}) (1)	(2)	(3)
0007+332(1)......	−400.7(1.3)	−41.5(1.3)	317.7(1.3)
(2)......	−405.6(0.3)	−46.3(1.0)	313.0(2.1)
0017+257(1)......	−426.8(10.3)	−67.6(3.8)	291.6(17.4)
2153+377(1)......	−349.2(36.4)	7.8(2.2)	364.8(32.0)
(2)......	−344.7(37.8)	10.9(1.8)	366.6(30.6)
2239+333(1)......	−200.2(3.1)	158.7(16.8)	...
2251+379(1)......	−496.5(13.7)	−137.0(1.3)	222.5(13.9)
(2)......	−485.9(5.6)	−126.5(8.3)	232.8(22.0)
2349+327(1)......	−421.0(2.8)	−61.7(1.6)	297.5(0.5)
(2)......	−422.7(0.8)	−63.5(0.3)	295.7(1.5)
(3)......	−424.6(2.2)	−65.5(1.1)	293.7(0.6)
2353+283(1)......	−449.4(2.1)	−90.2(1.0)	269.1(0.7)
2117+605(1)......	−344.3(11.4)	14.2(2.5)	372.8(16.2)
(2)......	−439.3(8.8)	−79.8(5.7)	279.7(19.1)
1753−113(1)......	−200.9(6.9)	161.7(7.0)	...
(2)......	−197.4(15.9)	166.1(2.0)	...
1954+331(1)......	−362.3(13.9)	−2.4(2.0)	357.5(13.6)

[a] Within the range $-500 < \mathrm{RM} < 500$ rad m^{-2}, possible values are labeled by (1), (2), and (3) and are listed in order of increasing RM. Uncertainties are in parentheses. The goodness of fit can be judged from the given uncertainties.

pairs have been plotted, that is, for sources 1323+370 and 2349+327 the third component-pair is not represented by a point in the figure. Also shown are data representing RM variations on angular scales of degrees for Region 1 and the NGP as computed and discussed in Paper I. We have not attempted to compute values for intersource variations from our observations since most of our absolute RM values are ambiguous or already included in the data from Paper I.

To investigate variations in Faraday rotation within the Galaxy we want to ignore those sources where it can be demonstrated that intrinsic Faraday rotation dominates the derived ΔRM. As discussed by Vallée (1980) and Simard-Normandin and Kronberg (1980) sources of large fractional polarization or which show little Faraday depolarization (as evidenced by nearly constant fractional polarization percentage with increasing λ) should have small internal rotation measures. To obtain a quantitative value indicative of the amount of internal Faraday rotation within our source components we calculated $m(L)/m(C) = m(1375\ \mathrm{MHz})/m(4885.1\ \mathrm{MHz})$ (see Table 1). A value near unity is consistent with little intrinsic Faraday depolarization, and by implication, little intrinsic contribution to the observed RM toward the source. A small value of $m(L)/m(C)$ implies a large depolarization with increasing wavelength. It is possible that $m(C)$ is overestimated relative to $m(L)$, making $m(L)/m(C)$ underestimated, since both the L and C band observations were made in the same array configuration, and polarized intensity maps generally show more clumping than total intensity maps of extragalactic sources (e.g., Spangler, Myers, and Pooge 1984). As is clear from Table 1, most of our sources have $m(L)/m(C) \approx 1$, while only a few have components with $m(L)/m(C) < 0.5$. One source (2106+494) has a component (labeled by [2] in Table 1) with $m(L)/m(C) = 0.24$, and this source has a high ΔRM. However, it is not clear whether to attribute this ΔRM to intrinsic effects since another source (1241+166 component [2]) has $m(L)/m(C) = 0.3$, yet a small ΔRM. It may be that only $m(L)/m(C)$ approaching zero is grounds for dismissing a source as dominated by intrinsic Faraday rotation. It is also possible that the line-of-sight Faraday rotation may have a significant contribution due to a screen near a source (i.e., not within our Galaxy), but since RMs for virtually all sources seen toward the Galactic poles are small, this circumstance is rare. We have plotted all ΔRM results.

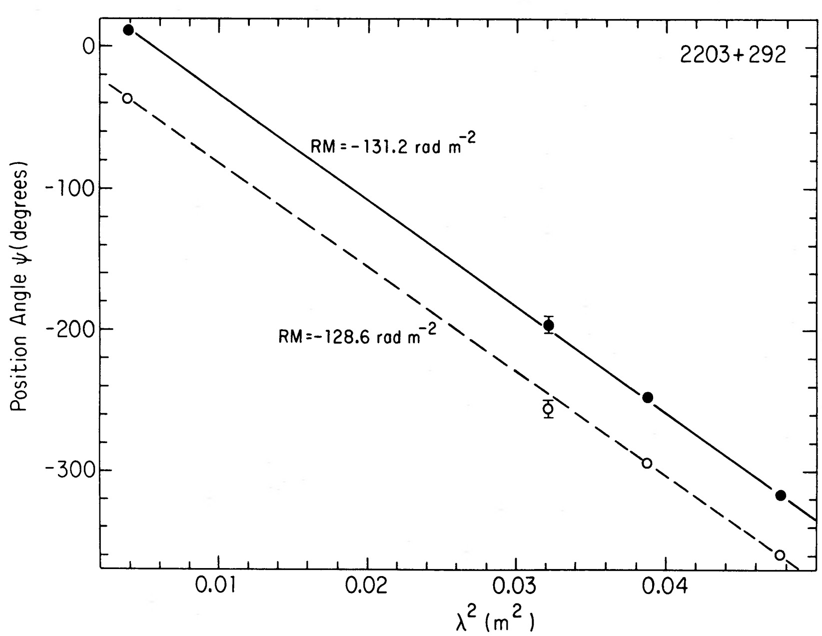

FIG. 5.—Linear fit to the observed position angles versus λ^2 for 2203+292. Open circles and filled circles are data points for component 1 and component 2, respectively. Where error bars are not shown, they are smaller than the displayed point size.

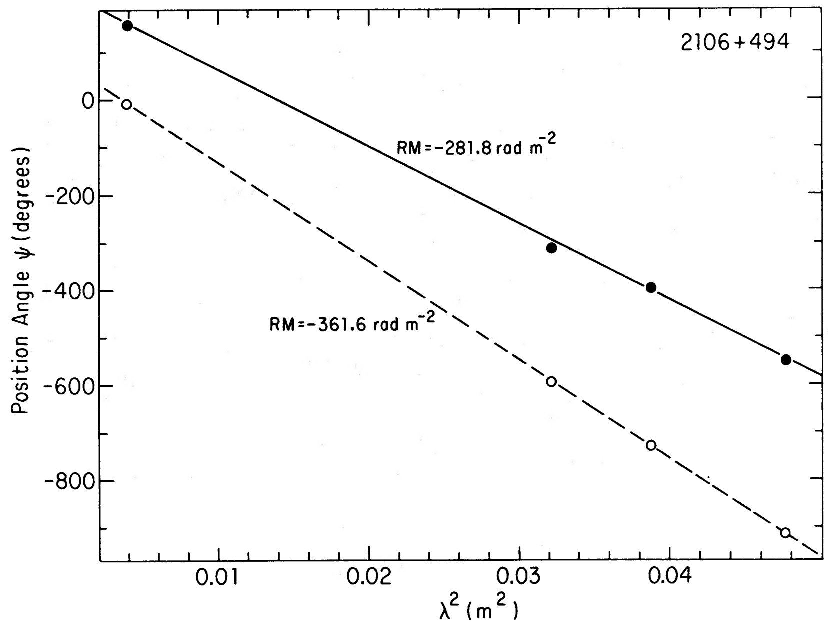

FIG. 6.—Same as Fig. 5 for source 2106+494

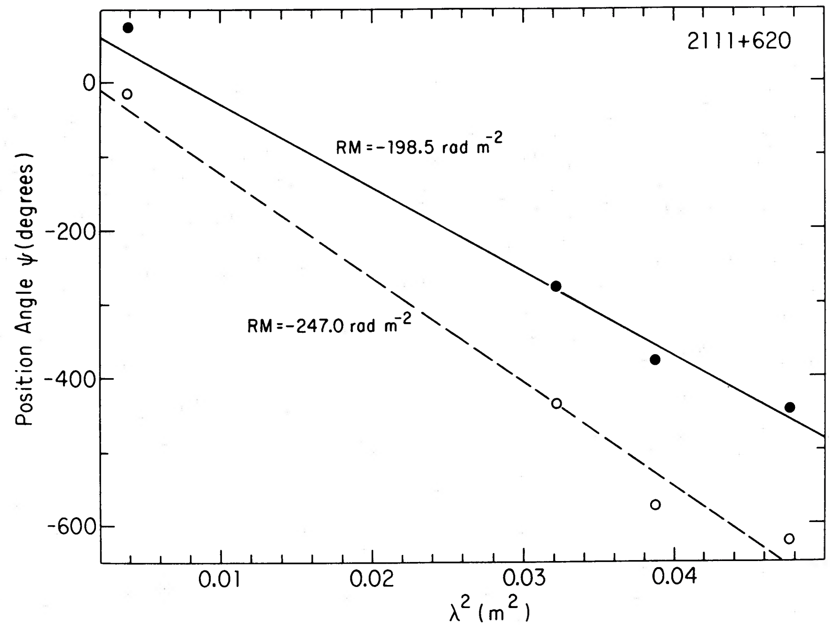

FIG. 7.—Same as Fig. 5 for source 2111+620

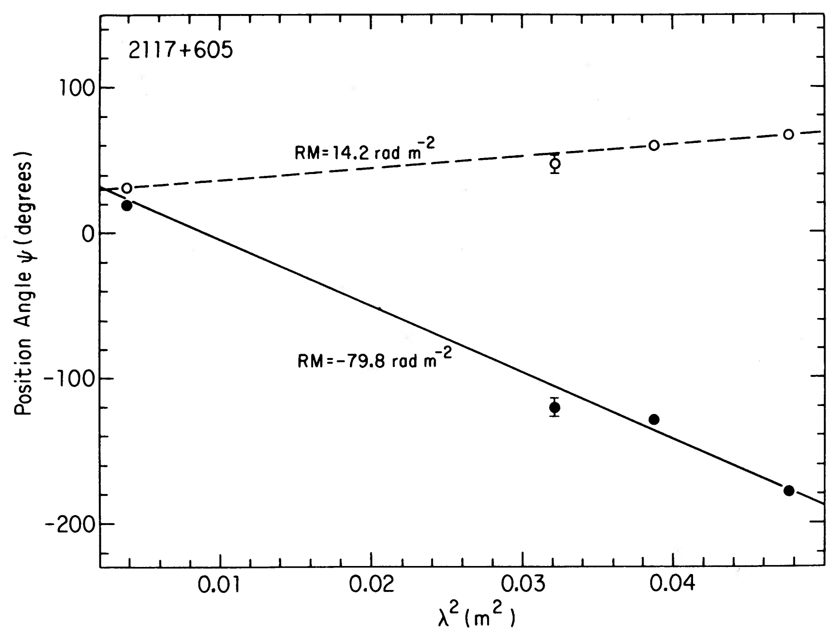

FIG. 8.—Same as Fig. 5 for source 2117+605. The lowest magnitude RMs from the list of possible values for this source were chosen for display.

TABLE 4

SOURCE PARAMETERS[a]

Source	4885.1 MHz			1675 MHz			1525 MHz			1375 MHz		
	I_{tot}^{peak} (mJy beam^{-1})	I_{pol}^{peak} (mJy beam^{-1})	ψ (°)	I_{tot}^{peak} (mJy beam^{-1})	I_{pol}^{peak} (mJy beam^{-1})	ψ (°)	I_{tot}^{peak} (mJy beam^{-1})	I_{pol}^{peak} (mJy beam^{-1})	ψ (°)	I_{tot}^{peak} (mJy beam^{-1})	I_{pol}^{peak} (mJy beam^{-1})	ψ (°)
1218+339(1) ...	576(24)	87.9(2.9)	−87.0(1.0)	1580(56)	201(4.4)	88.9(6.0)	1700(60)	152(4.7)	−83.3(0.9)	1920(67)	144(4.4)	−83.5(0.9)
1232+216(1) ...	40(7)	12.1(1.0)	−11.8(2.4)	...	...	...	104(19)	38.1(3.1)	−19.0(2.3)	125(19)	46.6(3.6)	−21.7(2.2)
(2) ...	59(7)	4.6(0.6)	26.7(3.7)	...	...	...	192(18)	22.2(1.8)	19.6(2.3)	236(21)	26.4(2.2)	14.7(2.4)
(1−2) ...	...	...	−38.5(4.4)	...	...	...	...	...	−38.6(3.3)	...	...	−36.4(3.3)
1241+166(1) ...	265(21)	10.5(0.8)	−55.3(2.2)	...	...	...	670(59)	25.2(1.3)	−78.1(1.5)	750(64)	28.3(1.3)	−81.9(1.3)
(2) ...	364(21)	20.4(0.8)	−31.0(1.1)	...	...	...	1250(59)	24.9(1.3)	−42.8(1.5)	1360(64)	21.9(1.3)	−56.5(1.7)
(1−2) ...	...	...	−24.3(2.5)	...	...	...	...	...	−35.3(2.1)	...	...	−25.4(2.1)
1251+278(1) ...	92(3)	13.4(0.3)	1.5(0.6)	205(4)	23.4(0.3)	8.3(6.0)	204(7)	29.6(0.4)	15.5(0.4)	221(6)	30.5(0.5)	15.8(0.5)
(2) ...	11(3)	2.0(0.3)	−29.3(4.3)	45(4)	3.7(0.3)	−34.3(6.4)	48(7)	4.5(0.4)	−10.9(2.5)	55(6)	5.8(0.5)	−22.8(2.5)
(1−2) ...	...	...	30.8(4.3)	...	...	42.6(2.3)	...	...	26.4(2.5)	...	...	38.6(2.5)
1308+227(1) ...	14(6)	2.8(0.5)	28.8(5.1)	79(4)	13.6(0.6)	14.9(6.1)	117(5)	18.5(0.6)	20.5(0.9)	120(5)	19.7(0.7)	19.9(1.0)
(2) ...	90(6)	10.6(0.5)	−76.5(1.4)	275(4)	40.7(0.6)	−87.6(6.0)	293(5)	37.0(0.6)	−79.9(0.5)	339(5)	38.9(0.7)	−79.5(0.5)
(1−2) ...	...	...	−74.7(5.3)	...	...	−77.5(1.4)	...	...	−79.6(1.0)	...	...	−80.6(1.1)
1323+370(1) ...	33(10)	5.9(0.9)	72.3(4.4)	104(17)	15.5(1.4)	76.0(6.5)	102(19)	17.6(1.8)	84.3(2.9)	99(21)	20.0(1.9)	88.6(2.7)
(2) ...	53(10)	9.8(0.9)	−25.0(2.6)	131(17)	18.0(1.4)	−17.9(6.4)	157(19)	23.1(1.8)	−14.5(2.2)	185(21)	23.6(1.9)	−17.0(2.3)
(3) ...	54(10)	8.2(0.9)	−1.5(3.1)	113(17)	16.8(1.4)	6.0(6.5)	105(19)	19.8(1.8)	10.1(2.6)	100(21)	23.1(1.9)	8.3(2.4)
(1−2) ...	...	...	−82.7(5.1)	...	...	−86.1(3.4)	...	...	−81.2(3.6)	...	...	−74.4(3.5)
(2−3) ...	...	...	−23.5(4.0)	...	...	−23.9(3.3)	...	...	−24.6(3.4)	...	...	−25.3(3.3)
(1−3) ...	...	...	73.8(5.4)	...	...	70.0(3.5)	...	...	74.2(3.9)	...	...	80.3(3.6)
0007+332(1) ...	35(1)	2.2(0.2)	−54.0(2.6)	...	...	...	98(2)	8.3(0.5)	43.0(1.7)	107(2)	8.4(0.6)	21.9(2.0)
(2) ...	58(1)	9.8(0.2)	82.4(0.6)	...	...	...	198(2)	33.6(0.5)	−8.4(0.4)	215(2)	34.8(0.6)	−34.5(0.5)
(1−2) ...	...	...	43.6(2.7)	...	...	...	...	...	51.4(1.7)	...	...	56.4(2.1)
0017+257(1) ...	45(6)	5.5(0.3)	21.0(1.6)	187(3)	16.8(0.9)	82.1(6.2)	197(3)	23.2(0.5)	70.6(0.6)	206(3)	25.4(0.8)	30.7(0.9)
2153+377(1) ...	432(8)	...	...	1580(9)	70.3(2.7)	37.5(6.1)	1710(21)	66.4(1.8)	37.6(0.8)	2050(9)	99(3)	41.7(0.8)
(2) ...	524(8)	...	...	1870(9)	82.2(2.7)	37.5(6.1)	2090(21)	79.4(1.8)	36.9(0.6)	2370(9)	116(3)	42.6(0.7)
(1−2) ...	...	...	...	...	...	0.0(1.4)	...	...	0.7(1.0)	...	...	−0.9(1.1)
2203+292(1) ...	327(5)	55.2(0.3)	−36.6(0.2)	793(10)	74.9(0.7)	−76.0(6.0)	850(16)	88.3(0.9)	65.6(0.3)	969(8)	90.7(0.5)	1.0(0.2)
(2) ...	131(5)	19.4(0.3)	12.2(0.4)	394(10)	38.6(0.7)	−16.3(6.0)	415(16)	50.6(0.9)	−67.6(0.5)	504(8)	63.5(0.5)	43.3(0.2)
(1−2) ...	...	...	−48.8(0.4)	...	...	−59.7(0.6)	...	...	−46.8(0.6)	...	...	−42.3(0.3)

TABLE 4—*Continued*

Source	4885.1 MHz			1675 MHz			1525 MHz			1375 MHz		
	I_{tot}^{peak} (mJy beam^{-1})	I_{pol}^{peak} (mJy beam^{-1})	ψ (°)	I_{tot}^{peak} (mJy beam^{-1})	I_{pol}^{peak} (mJy beam^{-1})	ψ (°)	I_{tot}^{peak} (mJy beam^{-1})	I_{pol}^{peak} (mJy beam^{-1})	ψ (°)	I_{tot}^{peak} (mJy beam^{-1})	I_{pol}^{peak} (mJy beam^{-1})	ψ (°)
2239+333(1) ...	153(22)	25.7(3.0)	−72.1(3.3)	442(18)	48.2(1.5)	−47.8(6.1)	503(20)	61.8(1.9)	64.1(0.9)	569(23)	53.1(1.7)	−36.4(0.9)
2244+366(1) ...	442(74)	15.1(3.0)	−88.8(5.7)	877(39)	49.1(2.0)	54.4(6.1)	967(44)	19.7(1.0)	−44.6(1.5)	1040(47)	20.6(1.0)	13.7(1.4)
(2) ...	282(74)	17.9(3.0)	70.1(4.8)	518(39)	30.8(2.0)	74.9(6.3)	557(44)	21.4(1.0)	1.3(1.3)	630(47)	20.9(1.0)	63.4(1.4)
(1−2) ...	...	...	21.1(7.5)	...	...	−20.5(2.2)	...	...	−45.9(2.0)	...	...	−49.7(2.0)
2251+379(1) ...	19(2)	1.9(0.2)	36.7(3.0)	69(4)	6.4(0.5)	−4.8(6.4)	73(5)	8.5(0.4)	−55.6(1.3)	89(5)	10.4(0.5)	53.2(1.4)
(2) ...	106(2)	5.5(0.2)	−25.2(1.0)	307(4)	12.3(0.5)	−75.6(6.1)	344(5)	16.4(0.4)	81.0(0.7)	385(5)	16.2(0.5)	18.1(0.9)
(1−2) ...	...	...	61.9(3.2)	...	...	70.8(2.5)	...	...	43.4(1.5)	...	...	35.1(1.7)
2349+327(1) ...	44(4)	5.5(0.2)	58.6(1.0)	...	...	...	111(9)	14.3(0.5)	−67.6(1.0)	125(9)	13.7(0.5)	85.2(1.0)
(2) ...	58(4)	11.0(0.2)	56.8(0.5)	...	...	...	110(9)	24.5(0.5)	−69.4(0.6)	118(9)	26.5(0.5)	77.4(0.5)
(3) ...	44(4)	4.6(0.2)	−78.4(1.2)	...	...	...	119(9)	15.6(0.5)	−31.3(0.9)	146(9)	15.4(0.5)	−61.9(0.9)
(1−2) ...	...	...	1.8(1.1)	...	...	...	...	...	1.8(1.2)	...	...	7.8(1.1)
(2−3) ...	...	...	−44.8(1.3)	...	...	...	...	...	−38.1(1.1)	...	...	−40.7(1.0)
(1−3) ...	...	...	−43.0(1.6)	...	...	...	...	...	−36.3(1.3)	...	...	−32.9(1.3)
2353+283(1) ...	181(10)	10.5(0.5)	−45.2(1.4)	...	...	...	475(25)	31.1(1.4)	−47.1(1.3)	498(26)	30.1(1.4)	89.5(1.3)
2106+494(1) ...	165(36)	26.2(3.4)	−6.9(3.7)	327(27)	56.2(1.0)	−55.4(6.0)	365(31)	73.2(2.4)	−9.6(0.9)	432(34)	82.0(2.4)	−13.9(0.8)
(2) ...	264(36)	28.7(3.4)	−19.9(3.4)	702(27)	37.6(1.0)	47.1(6.1)	782(31)	33.5(2.4)	−37.4(2.1)	876(34)	22.9(2.4)	−11.3(3.0)
(1−2) ...	...	...	13.0(5.0)	...	...	77.5(0.9)	...	...	27.8(2.2)	...	...	−2.6(3.1)
2111+620(1) ...	415(71)	12.2(1.7)	−14.1(4.0)	1060(48)	8.4(1.0)	−76.1(6.9)	1220(54)	14.3(1.3)	−34.9(2.6)	1350(60)	22.0(1.9)	−82.0(2.5)
(2) ...	201(71)	8.8(1.7)	75.9(5.5)	520(48)	19.3(1.0)	82.1(6.2)	530(54)	20.8(1.3)	−17.3(1.8)	630(60)	32.6(1.9)	−84.6(1.7)
(1−2) ...	...	...	90.0(6.8)	...	...	21.8(3.7)	...	...	−17.6(3.2)	...	...	2.6(3.0)
2117+605(1) ...	153(10)	76.2(1.5)	30.9(0.6)	434(21)	135(1.5)	46.6(6.0)	481(19)	154(1.6)	59.4(0.3)	502(18)	165(1.2)	66.6(0.2)
(2) ...	150(10)	13.0(1.5)	19.4(3.3)	402(21)	21.7(1.5)	59.1(6.3)	445(19)	29.1(1.6)	50.4(1.6)	507(18)	32.8(1.2)	1.6(1.0)
(1−2) ...	...	...	11.5(3.4)	...	...	−12.5(2.0)	...	...	9.0(1.6)	...	...	65.0(1.0)
2117+494(1) ...	155(54)	16.7(4.3)	73.2(7.4)	449(45)	66.4(4.3)	−28.5(6.3)	510(52)	74.6(4.7)	−58.0(1.8)	601(59)	91.8(5.8)	−40.7(1.8)
(2) ...	399(54)	36.6(4.3)	−58.4(3.4)	1220(45)	118(4.3)	−69.4(6.1)	1400(52)	134(4.7)	57.1(1.0)	1590(59)	167(5.8)	42.3(1.0)
(1−2) ...	...	...	−48.4(8.1)	...	...	40.9(2.1)	...	...	64.9(2.1)	...	...	−83.0(2.1)
1753−113(1) ...	84(27)	5.7(1.6)	−41.9(8.0)	188(17)	11.2(1.5)	14.4(7.1)	237(19)	10.6(1.2)	−84.7(3.2)	256(20)	10.8(1.2)	−1.7(3.2)
(2) ...	120(27)	8.3(1.6)	5.9(5.5)	285(17)	17.5(1.5)	−79.5(6.5)	361(19)	26.5(1.2)	−24.1(1.3)	384(20)	27.1(1.2)	61.8(1.3)
(1−2) ...	...	...	−47.8(9.7)	...	...	−86.1(4.5)	...	...	−60.6(3.5)	...	...	−63.5(3.5)
1954+331(1) ...	98(14)	3.6(0.7)	24.5(5.6)	242(8)	6.6(0.5)	18.8(6.4)	281(10)	11.2(0.5)	15.9(1.3)	315(10)	12.9(0.6)	16.2(1.3)

[a] Tabulated are values of the total intensity, linearly polarized intensity, and position angle at the peak of polarized intensity for each component where the polarization percentage is greater than 1%–2%. All uncertainties are shown in parentheses. The components correspond to and have the same labels as those in Table 1. Also shown are the differences in position angle for each pair of components within a source. Note that all position angles are specified such that they lie within ±90°. Position angles at 1675 MHz have been corrected as discussed in § III*b*. Interference at 1675 MHz caused us to discard the data for many sources. In all cases circular beams were used to produce the final maps with pixel sizes of 1 arcsec^2, where the half-power beamwidths for each source were as follows: 1218+339, 4″.75; 1232+216, 6″.1; 1241+166, 6″.5; 1251+278, 5″.0; 1308+277, 7″.8; 1323+370, 7″.5; 0007+332, 9″.0; 0017+257, 12″.5; 2153+377, 6″.0; 2203+292, 5″.5; 2239+333, 5″.0; 2244+366, 5″.4; 2251+379, 6″.0; 2349+327, 8″.8; 2353+283, 7″.5; 2106+494, 4″.5; 2111+620, 5″.0; 2117+605, 5″.5; 2117+494, 4″.75; 1753−113, 6″.5; 1954+331, 4″.5.

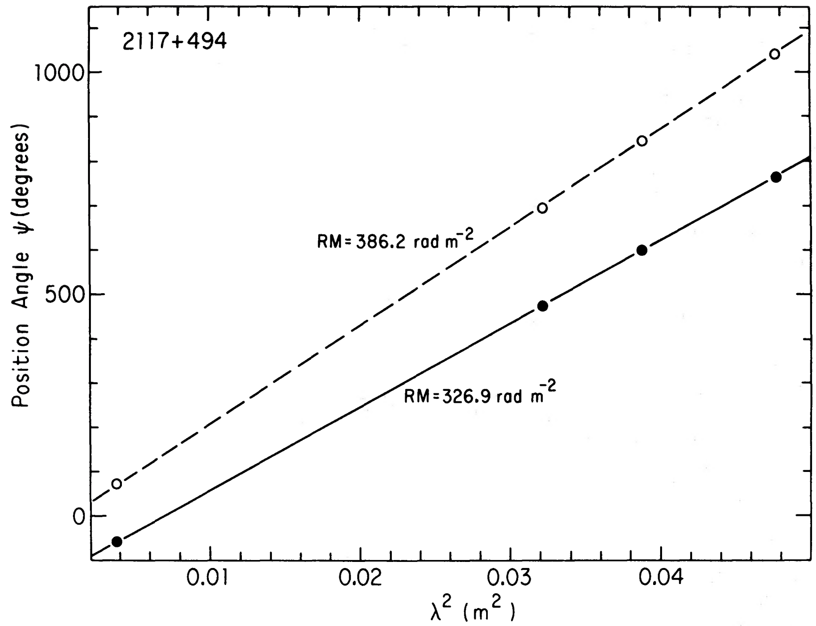

FIG. 9.—Same as Fig. 5 for source 2117+494

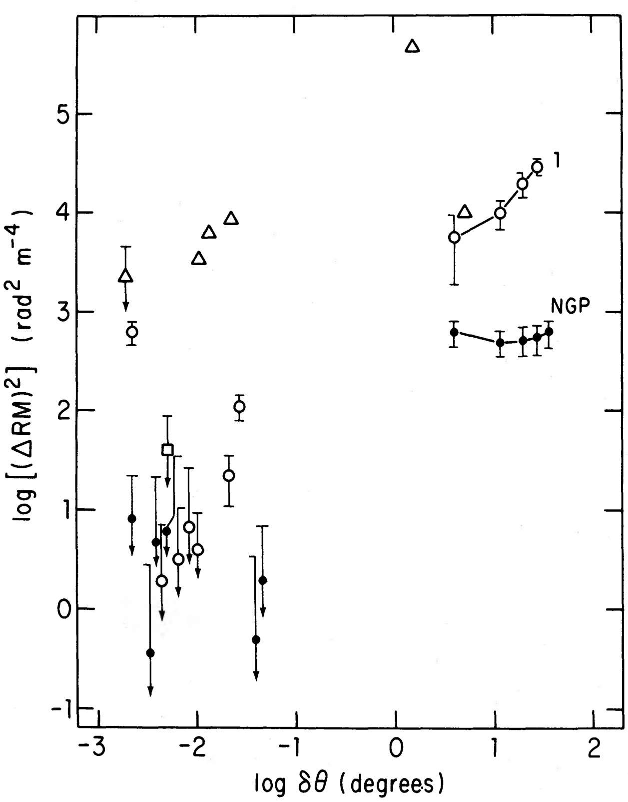

FIG. 10.—Plot of $(\Delta\mathrm{RM})^2$ vs. component separation for the observed extended sources (compare with Fig. 3 of Paper I). Filled circles represent values for sources seen in the North Galactic Pole region; open circles for Region 1 (defined in the text); open triangles for sources at $l^{\mathrm{II}} \approx 90°$, $b^{\mathrm{II}} \approx 0°$; the open square is a point for the one source at another galactic longitude, and within the plane, for which a ΔRM was obtainable. The two open triangles at $\delta\theta > 1°$ are from differences between three sources near $L^{\mathrm{II}} \approx 90°$, $b^{\mathrm{II}} \approx 0°$, for which RM values are taken from Simard-Normandin, Kronberg, and Button (1981); see text. Points at $\delta\theta > 1°$, connected by lines and labeled by "NGP" and Region "1" are averages of squared differences of integrated RM values for all possible pairs of extragalactic sources from Simard-Normandin, Kronberg, and Button (1981) with separations within small $\delta\theta$ bins (see Paper I).

The general behavior of $(\Delta\mathrm{RM})^2$ for our observed sources in Region 1 and the NGP is entirely consistent with the earlier results for a few double sources taken from the literature and presented in Paper I. Most of the data strongly support the case stated in Paper I that variations in RM can be used to determine a structure function which is consistent with a power-law power spectrum for variations in $(n_e \boldsymbol{B})$ of exponent $\alpha \approx -3.1 \pm 0.6$. An outer scale for such a spectrum appears to be near $\sim 5°$ or $\lesssim 90$ pc at a distance of 1 kpc. It is not at present clear what lower limit can be set for the angular scale at which RM variations (and therefore at what linear scale magnetic field variations) will disappear.

Most interestingly, the results for each one of the four sources (2106+494, 2111+620, 2117 + 605, and 2117+494) in the Galactic plane at $l^{\mathrm{II}} \approx 90°$, show unexpectedly high $(\Delta\mathrm{RM})^2$ in comparison with NGP and Region 1 sources. Clearly more sources in this area of the sky must be observed to obtain better statistics. Only three sources are listed by Simard-Normandin, Kronberg, and Button (1980) for a region along the galactic plane ($|b^{\mathrm{II}}| < 10°$) of approximately $\pm 30°$ centered on $l^{\mathrm{II}} \approx 90°$. These sources (2037+51 RM = -258, 2106+49 RM = -359, 2117+49 RM = $+347$ rad m^{-2}) have RMs apparently dominated by Faraday rotation within our Galaxy, according to Simard-Normandin and Kronberg (1980). The large differences among the RMs for these three sources are represented by the two open triangles plotted at large $\delta\theta$ in Figure 10. Note these two points are indicative of RM variations larger than for Region 1 or the NGP at large angular separations, consistent with the larger $(\Delta\mathrm{RM})^2$ at small angular scales as well.

Perhaps there is a large probability for lines of sight along the Galactic plane to encounter regions of enhanced turbulence. Such circumstances might explain the large RM variations seen at $l^{\mathrm{II}} \approx 90°$, but we have not presently examined enough rotation measures of double sources at other directions through the plane. Besides the sources at $l^{\mathrm{II}} \approx 90°$, the only small galactic latitude source with two detectable polarized components (1753−113) has a small ΔRM.

At present, there is some limited evidence to suggest that the line of sight toward $l^{\mathrm{II}} \approx 90°$, $b^{\mathrm{II}} \approx 0°$ is special. A single localizable object is probably not the cause of the high $(\Delta\mathrm{RM})^2$ values for the four sources observed in this direction. A number of large, diffuse H II regions (S129, IC 1396), dark clouds, and a supernova remnant (DA 530) lie in the Galactic plane in this direction, but it is not readily apparent that these features are important, especially since none of them actually lie in front of any of the four sources with high $(\Delta\mathrm{RM})^2$. If one such feature is responsible for the enhanced turbulence it would have to be large in angular extent, since the four high $(\Delta\mathrm{RM})^2$ are grouped in two pairs separated by $\sim 10°$ on the sky. More important may be the presence of Region A of Simard-Normandin and Kronberg (1980) centered at $l^{\mathrm{II}} \approx 90°$, $b^{\mathrm{II}} \approx -30°$ and bounded roughly by the galactic plane at $70° \lesssim l^{\mathrm{II}} \lesssim 130°$.

Rotation measures for extragalactic sources seen in Region A are generally large and negative at ~ -150 rad m^{-2}. The few pulsars seen in this general direction also have negative RMs near -40 rad m^{-2}. Using dispersion measure distances to these pulsars Simard-Normandin and Kronberg conclude, for moderate assumptions for the electron density and magnetic field strength in the region, that Region A is a Galactic feature at $\gtrsim 3$ kpc distance and of roughly 2 kpc size. It is the contention of Vallée (1984) that Region A is a "magnetic bubble," the evacuation of gas and magnetic fields from the cavity possibly caused by supernovae or stellar winds from a young stellar association. He discusses four possible bubbles in the local interstellar medium of which Region A is the largest in angular extent. If this picture is correct, we might expect some jumbling of the magnetic field at the boundary between the bubble and the Galactic plane. At this time these conjectures can only point to the need for further observations directed at learning more about RM variations in the Galactic plane, especially at $l^{\mathrm{II}} \approx 90°$, and certainly more work on explaining the nature of Region A.

The authors are particularly grateful to S. R. Spangler for his input during the formative stages of this work, and for his comments on an early draft of this paper. We also wish to thank the staff of the National Radio Astronomy Observatory for their support. In particular, we thank Robert Hill for calibrating the data in our absence. The National Radio Astronomy Observatory is operated by Associated Universities, Inc., under contract with the National Science Foundation. This research was supported by the National Astronomy and Ionosphere Center which is operated by Cornell University under contract with the National Science Foundation.

REFERENCES

Armstrong, J. W., Cordes, J. M., and Rickett, B. J. 1981, *Nature*, **291**, 561.
Cordes, J. M., Weisberg, J. M., and Boriakoff, V. 1985, *Ap. J.*, **228**, 221.
Higdon, J. C. 1984, *Ap. J.*, **285**, 109.
McIvor, I. 1977*a M.N.R.A.S.*, **178**, 85.
———. 1977*b*, *M.N.R.A.S.*, **179**, 13.
Rickett, B. J., Coles, W. A., and Bourgois, G. 1984, *Astr. Ap.*, **134**, 390.
Ruzmaikin, A. A., and Shukurov, A. M. 1982, *Ap. Space Sci.*, **82**, 397.
Simard-Normandin, M., and Kronberg, P. P. 1980, *Ap. J.*, **242**, 94.
Simard-Normandin, M., Kronberg, P. P., and Button, S. 1981, *Ap. J. Suppl.*, **45**, 97.
Simonetti, J. H., Cordes, J. M., and Spangler, S. R. 1984, *Ap. J.*, **284**, 126 (Paper I).
Spangler, S. R., Myers, S. T., and Pooge, J. J. 1984, *A.J.*, **89**, 1478.
Vallée, J. P. 1980, *Astr. Ap.*, **86**, 251.
———. 1983, *Astr. Ap. Suppl.*, **51**, 127.
———. 1984, *Astr. Ap.*, **136**, 373.

JAMES M. CORDES: Space Sciences Building, Cornell University, Ithaca, NY 14853

JOHN H. SIMONETTI: National Radio Astronomy Observatory, Edgemont Road, Charlottesville, VA 22903